Negative Magnus Forces in the Critical Reynolds Number Regime

CLIVE A. J. FLETCHER*
Australian Defence Scientific Service, Department of Supply, Weapons Research Establishment, Salisbury, South Australia.

A spinning two-dimensional cylinder experiences a negative Magnus lift force at small spin ratios (peripheral speed/freestream speed) in the critical Reynolds number regime in steady incompressible flow. A comprehensive explanation of this phenomenon is offered. A negative Magnus side force at a small spin ratio has been measured on an inclined, spinning ogive-cylinder at a certain subcritical cross-flow Reynolds number. Through use of the impulsive flow analogy, the two-dimensional explanation can be applied to the negative side force experienced by the inclined spinning ogive-cylinder if the effect of the body vortices is allowed for. At both critical and subcritical cross-flow Reynolds numbers, the body vortices produce a side force which is opposed to, and larger than, the side force associated with the cross-flow separation positions. The cross-flow separation positions are similar to those on a spinning two-dimensional cylinder. Starting with the measured separation and body vortex positions, a simple potential flow model is developed, which predicts total side forces in qualitative agreement with those measured.

Nomenclature

C_D = two-dimensional drag coefficient
C_L = two-dimensional lift coefficient
C_N = side moment coefficient
C_P = pressure coefficient, $(P - P_\infty)/\frac{1}{2}.\rho.U^2{}_\infty$
C_Y = total side force coefficient, $Y/\frac{1}{2}.\rho.U^2{}_\infty.S$
C_{YL} = local side force coefficient, $Y_L/\frac{1}{2}.\rho.(U_\infty.\sin\theta)^2.D$
D = diameter
i = $(-1)^2$
K = rate of discharge of circulation
k = proportion of circulation which penetrates the boundary layer
L = total body length
L_n = nose length
n = nose
P = pressure
Re = Reynolds number, $U_\infty.D/\nu$
Re_{cross} = cross-flow Reynolds number, $(U_\infty.D\sin\theta)/\nu$
r = radius of cylinder
S = model base area (coefficient reference area)
t = time
t_e = equivalent time (measured from the beginning of separation)
U_∞ = freestream velocity
U_{inner} = velocity at the inner edge of the shear layer
U_{outer} = velocity at the outer edge of the shear layer
u = velocity component parallel to the freestream [two-dimensional, defined by Eq. (4)]
v = velocity component perpendicular to the free stream [two-dimensional, defined by Eq. (4)]
W = complex potential
x = axial distance
x_e = equivalent axial distance (measured from the shoulder of the nose)
Y = total side force
Y_L = local side force
y = lateral vortex component
z = complex co-ordinate in two-dimensional flow, $x + iy$; normal vortex component
α = spin ratio (peripheral speed/freestream speed or cross-flow speed)
0 = vortex at the center of the cylinder
1 = upper vortex strength (see Fig. 9)
2 = lower vortex strength (see Fig. 9)
θ = angle of incidence
λ = proportion of discharged circulation which reaches the vortex
ν = kinematic viscosity
ρ = density
τ = nondimensional time, $U_\infty.t/r$
φ = roll angle
χ = force correction due to neglecting the term $z + 1/z$ in the wake region

Subscripts

1 = upper station in Fig. 9
2 = lower station in Fig. 9
sep = separation
∞ = freestream
$-$ = conjugate, as in $\bar{z} = x - iy$

Received November 1, 1971; revision received August 22, 1972.
Index categories: Subsonic and Transonic Flow; Jets, Wakes and Viscid-Inviscid Flow Interactions.

* Research Scientist, Aerospace Division; presently at Department of Mechanical Engineering, University of California, Berkeley, Calif.

Introduction

IN general, critical Reynolds number (10^5 to 5×10^5) effects are associated with marked changes in boundary-layer separation position. For the flow about a two-dimensional cylinder, the phenomenon is explained by Tani.[1] It is, perhaps, less well known that for an inclined slender axisymmetric body, a rearward shift in the cross-flow separation position occurs in the critical cross-flow Reynolds number range. The rearward shift in separation position causes a reduction in the drag and cross-flow drag, respectively.

If a two-dimensional cylinder, spinning anti-clockwise, is subjected to a steady flow from right to left, the usual result is an upwards Magnus lift force; conventionally this is called a positive Magnus lift force. The force arises as a result of the boundary layers separating asymmetrically. Under the condition of small spin ratio (peripheral speed/free-stream speed ≈ 0.2) in the critical Reynolds number range, the boundary layer on the advancing side of the cylinder separates further round the cylinder than does the boundary layer on the receding side; the net result is a negative Magnus lift force. This negative lift force was first described by Krahn[2] and has been extensively investigated by Swanson.[3]

If an inclined axisymmetric body is spun about its longitudinal axis in an anti-clockwise direction viewed from the rear, a side force is normally developed to the right (positive direction) due to the spin, cross-flow interaction. The present author, in investigating the Magnus characteristics of an inclined ogive-cylinder body,[4] measured a negative Magnus side force at a small spin ratio, but at a subcritical cross-flow Reynolds number.

In the present paper Tani's[1] explanation is extended to spinning cylinders and linked with Swanson's[3] results and some pressure distributions obtained on spinning two-dimensional cylinders by Griffiths and Ma.[5] It will be assumed that the explanation, although strictly only applicable to steady flow, can be applied to an impulsively started two-dimensional cylinder. Through use of the impulsive flow analogy,[6] the explanation can then be extended to inclined axisymmetric bodies in the critical cross-flow Reynolds number regime.

When the two-dimensional explanation is applied to the three-dimensional situation, it predicts separation point changes with Reynolds number which are supported by experiment.[7] It will be shown that, with the aid of a simple potential flow model, the discrepancy can be resolved if the influence of the body vortices is taken into account.

Two-Dimensional Results and Explanation

For a spinning two-dimensional cylinder, at small values of spin ratio (peripheral speed/freestream speed) in the critical Reynolds number region ($UD/\nu = 10^5$ to 5×10^5), Swanson[3] has measured a negative (downward) lift force (Fig. 1) and similar results have been obtained by Griffiths and Ma.[5]

For the flow of a uniform freestream about a nonspinning two-dimensional, circular cylinder operating in the critical Reynolds number regime, the boundary layer separates initially as a laminar boundary layer at approximately 82° from the front stagnation point. Transition occurs in the discharged boundary layer and the subsequent entrainment of fluid into the shear layer causes a lowering of pressure between the shear layer and the cylinder surface. If transition occurs close to the initial separation position, the pressure reduction is sufficient to cause reattachnemt of the separated shear layer to the cylinder surface as a turbulent boundary layer.[1] Subsequently, the turbulent boundary-layer separates at approximately 135° from the front stagnation point.

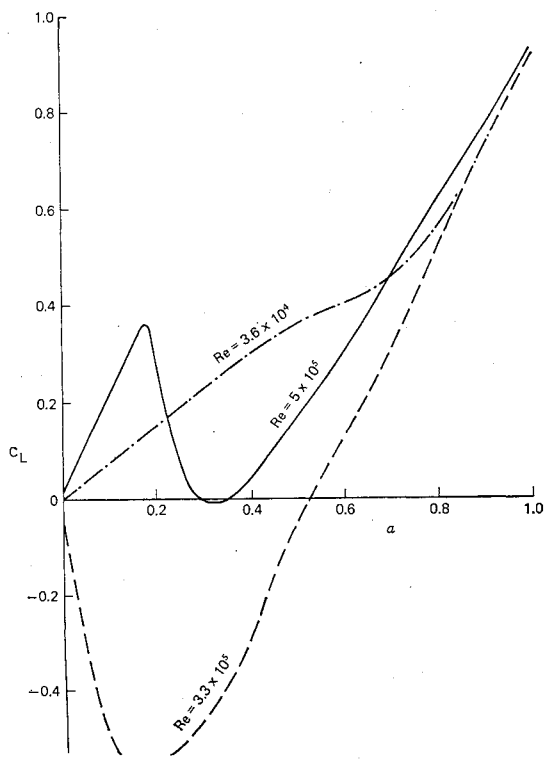

Fig. 1 Variation of two-dimensional magnus lift coefficient with spin ratio (from Ref. 3).

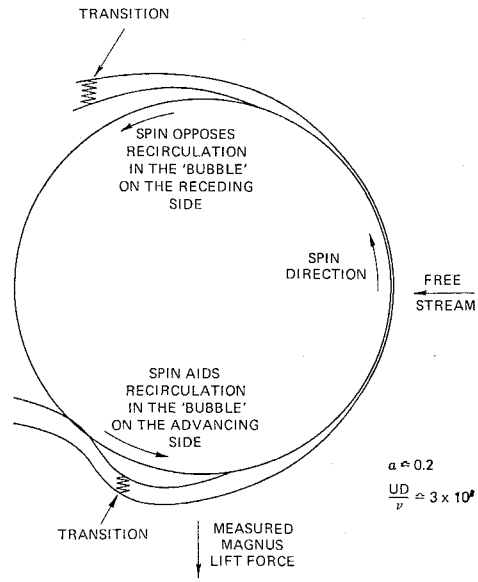

Fig. 2 Explanation of the negative magnus force.

It is apparent[1,5] that in the critical Reynolds number regime, the flow around a circular cylinder is characterized by a separation bubble in the boundary layer on each side. With increasing Reynolds number the point of transition advances upstream towards the separation point of the laminar boundary layer. At sufficiently high Reynolds number,[8] transition occurs before a laminar separation can take place, no bubble occurs and the turbulent boundary layer separates at about 110°.

For spinning, two-dimensional cylinders not operating in the critical Reynolds number regime, the effect of spin is to move the separation angle in the direction of spin. The associated asymmetric pressure distribution causes an upwards (positive) force. In the critical Reynolds number regime, the region of transition occurs close enough to the cylinder surface to be affected by the spin. Where the surface moves with the outer flow, transition is delayed, i.e. the boundary layer development is similar to that for a nonspinning cylinder at a lower Reynolds number. Conversely, where the cylinder surface moves against the outer flow, transition occurs closer to the separation point; i.e., the effective Reynolds number is increased. The differential movement of the position of transiton amplifies the differential extent of the separation bubbles. The general situation is shown in Fig. 2 for a Reynolds number of approximately 3×10^5 and a spin ratio of approximately 0.2.

Over the lower surface, transition occurs closer to the initial separation than for the nonspinning cylinder; thereafter, the shear layer reattaches, and subsequently the turbulent boundary layer finally separates. Associated with the predominantly attached flow prior to the final separation, is a

Table 1 Postulated boundary-layer separation characteristics for Fig. 1

	$\alpha = 0$		$\alpha = 0.1$		$\alpha = 0.3$		$\alpha = 0.8$	
Reynolds Number	Rec. side	Adv. side	Rec. side	Adv. side	Rec. side	Adv. side	Rec. side	Adv. side
3.6×10^4	L[a]	L	L	L	L	L	L	L/T[b]
3.3×10^5	L/T & B[c]	L/T & B	L	L/T & B	L	L/T	L	L/T
5×10^5	L/T & B	L/T & B	L/T & B	L/T & B	L	L/T	L	L/T

[a] L = Laminar.
[b] T = Turbulent.
[c] B = Laminar separation bubble.

low pressure region outside the boundary layer. Over the upper surface, transition occurs too far from the cylinder surface to cause reattachment. The pressure recovery after separation implies a region of relatively high pressure over the upper surface of the cylinder. The net effect is a lift force directed downwards. Measured pressure distribuions about a spinning cylinder[5] support the model shown in Fig. 2. For the results shown in Fig. 1(with the model shown in Fig. 2 in mind), it is suggested that the state of the separating boundary layers is as shown in Table 1.

Impulsive Flow Analogy

In order to apply the explanation of a two-dimensional phenomenon to a slender axisymmetric body at incidence, it is convenient to make use of the impulsive flow analogy.[6]

The impulsive flow analogy, which is illustrated in Fig. 3, states that the cross-flow behavior at any axial station a distance, $(x_e \cdot \tan\theta)/D$, downstream of the beginning of cross-flow separation is equivalent to the flow about an impulsively started two-dimensional cylinder at a time, Ut_e/D, after the beginning of separation. In the present paper, the beginning of cross-flow separation is taken as the base of the nose section. This was confirmed experimentally in Refs. 4 and 7, and is in agreement with the large incidence results of Ref. 9. The beginning of separation for the flow about an impulsively started two-dimensional cylinder is given by $Ut/D = 0.176$.[10]

If the impulsive flow analogy is to be used to link the results for the impulsively started two-dimensional cylinder to those for the three-dimensional body at incidence, then it is necessary to compare the variation of gross properties of the flow at the same Reynolds number (and Mach number if applicable) with nondimensional time (Ut_e/D) and nondimensional axial distance $[(x_e \cdot \tan\theta)/D]$. For the inclined three-dimensional body, the relevant Reynolds number is the cross-flow Reynolds number (i.e. based on the cross-flow velocity rather than the free stream velocity). The gross properties are typically the viscous normal force, the side force (if the model is spinning), the cross-flow separation angles and the co-ordinates and strength of the body vortices. The measurement of such data and the use of the impulsive flow analogy is indicated in Table 2.

The impulsive flow analogy has been applied most commonly to the viscous normal force for nonspinning slender bodies of revolution at high incidence[6,16] and some attempt has been made to develop the impulsive flow analogy rigorously.[23] If one postulates that the local side force coefficient C_{YL}, is a function of spin ratio, α, and axial position, $(x_e \cdot \tan\theta)/D$, it

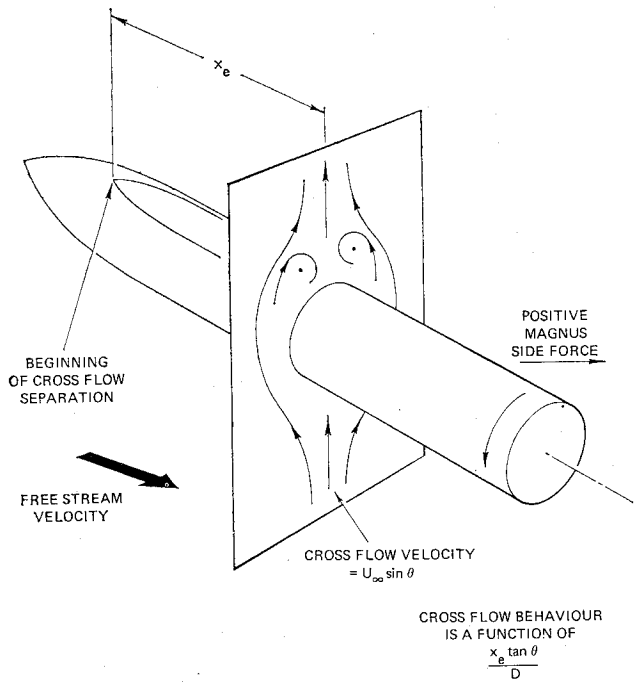

Fig. 3 The impulsive flow analogy.

can be shown[4] that the total side force coefficient C_Y is proportional to the integration of the local side force coefficient over the body length, with respect to $(x_e \cdot \tan\theta)/D$ at constant α.

In particular,

$$\frac{\tan\theta \cdot C_Y}{\sin^2\theta} = \frac{4}{\pi}\int_{\frac{L_n \cdot \tan\theta}{D}}^{\frac{L \cdot \tan\theta}{D}} C_{YL} \cdot d\left(\frac{x_e \cdot \tan\theta}{D}\right) \tag{1}$$

and

$$\frac{-C_N}{\cos^2\theta} = \frac{4}{\pi}\int_{\frac{L_n \cdot \tan\theta}{D}}^{\frac{L \cdot \tan\theta}{D}} C_{YL} \cdot \left(\frac{x_e \cdot \tan\theta}{D}\right) \cdot d\left(\frac{x_e \cdot \tan\theta}{D}\right) \tag{2}$$

where L_n is the nose length.

Thus by plotting the functions on the left-hand side of Eqs. (1) and (2) against $(x_e \cdot \tan\theta)/D$, the impulsive flow analogy can be used to compare bodies of differing lengths.

The variation of side force coefficient with spin ratio is shown at various Reynolds numbers, and for two body lengths in

Table 2 References relevant to the impulsive flow analogy

	Impulsively started two-dimensional flow		Flow about inclined axisymmetric body		Use of the impulsive flow analogy for correlation
	nonspinning	spinning	nonspinning	spinning	
Viscous normal force	11;		9[a],16[a];	4,7,20;	21;
Side force (spinning model)	—	15[b];	—	4,7,20;	15;
Cross-flow separation angles	15;	15;	7;	7;	15;
Position of body vortices	12,13,14, 15;	15;	9,16,17, 18,21;	4,7,20;	15,19;
Strength of body vortices	13;		9,16[c],17[c], 18,21;		19,21[d];

[a] From pressure distribution.
[b] Deduced from vortex and cross-flow separation positions.
[c] Deduced from normal force and vortex positions.
[d] Same authors[22] indicate vortex strengths can be correlated better, with vortex strengths behind cylinders in steady two-dimensional flow, if the array of vortices behind the inclined axisymmetric body is considered as a Karman vortex street that has been swept back in the flow direction by the mainstream.

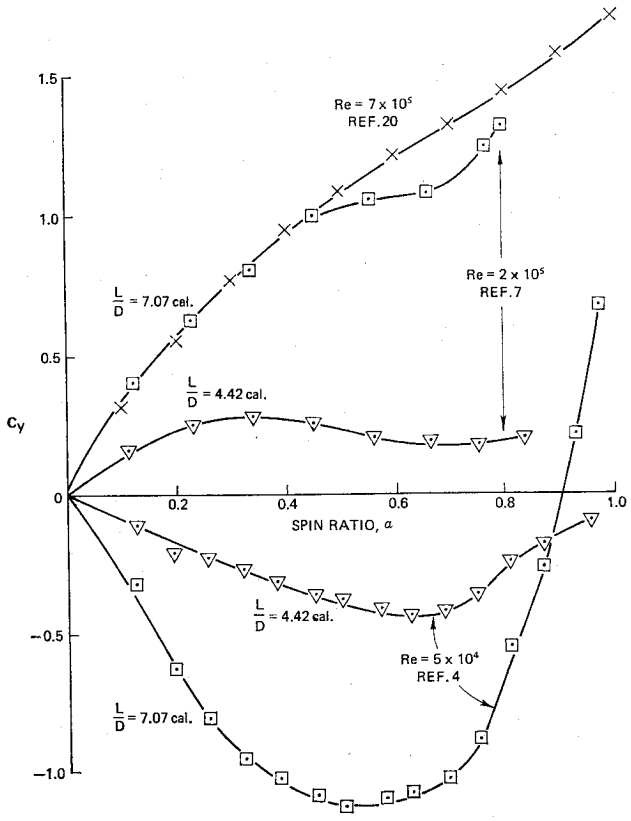

Fig. 4 Variation of side force coefficient with spin ratio, Reynolds number and body length on a spinning, ogive-cylinder at an incidence of 30°.

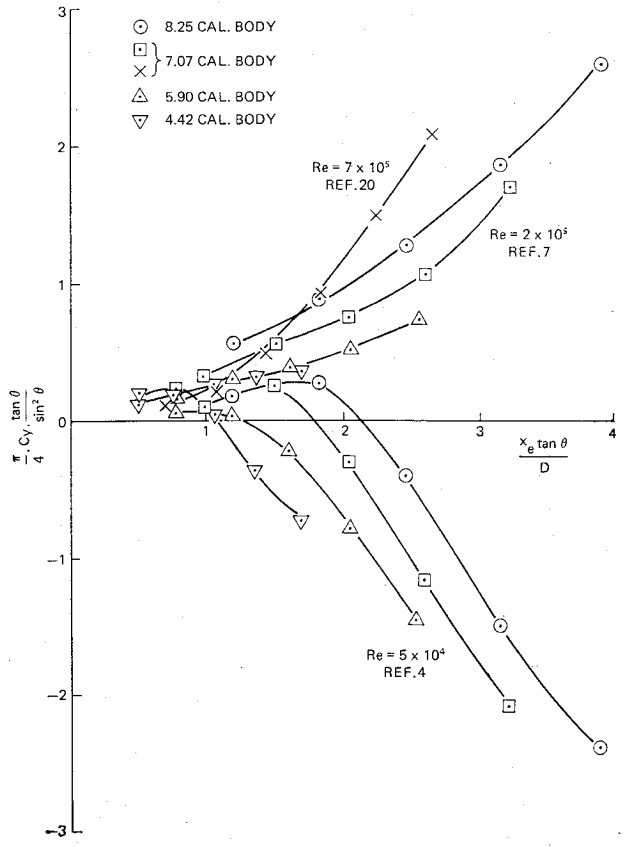

Fig. 5 Variation of modified side force coefficient with length parameter at different Reynolds numbers and a spin ratio of 0.5.

Fig. 4. These results are taken from Refs. 4, 7, and 20 and refer to a spinning inclined ogive-cylinder. They illustrate how wide the variation of side force is with model length. By making use of Eq. (1) above, the side force results can be replotted to show the variation with the parameter, $(x_e \cdot \tan\theta)/D$, at constant spin ratio, α. The results of this are presented in Fig. 5.

It is apparent that use of the impulsive flow analogy has caused considerable contraction of the results. At first sight one might expect all the results to lie on a single curve. Since, for each body length, each data point corresponds to a different incidence it also corresponds to a different cross-flow Reynolds number $(UD \sin\theta)/\nu$; thus a certain scatter is to be expected. It can be seen that when $UD/\nu = 5 \times 10^4$, at which the negative side forces occur, the family of curves grows out of the upper family, i.e. at small $(x_e \cdot \tan\theta)/D$ the results are positive for all Reynolds numbers.

A typical variation of body vortex positions with non-dimensional time and nondimensional distance along the slender body is shown in Fig. 6.[15] These results are for a spin ratio of 0.5 and compare vortex positions obtained from an impulsively started two-dimensional cylinder, $Re = 6 \times 10^3$, and from a tangent ogive-cylinder at cross-flow Reynolds numbers, $Re_{cross} = 1.5 \times 10^3 - 2.5 \times 10^4$. The agreement is reasonable at corresponding Reynolds numbers, particular at large values of Ut_e/D, $(x_e \cdot \tan\theta)/D$. On the side of the cylinder which is receding in the cross-flow direction, the results at $Re_{cross} = 2.5 \times 10^4$ are not in agreement with those at the lower Reynolds number. However, it is at precisely this condition that the negative Magnus force occurs. It will be shown later that the body vortices cause the negative Magnus force and, in particular, that the vortex, on the side where the cylinder is receding, has the greater effect.

Generally the body vortex positions can be correlated closely using the impulsive flow analogy in the spin ratio considered, i.e. $\alpha = 0$ to 1. The impulsive flow analogy

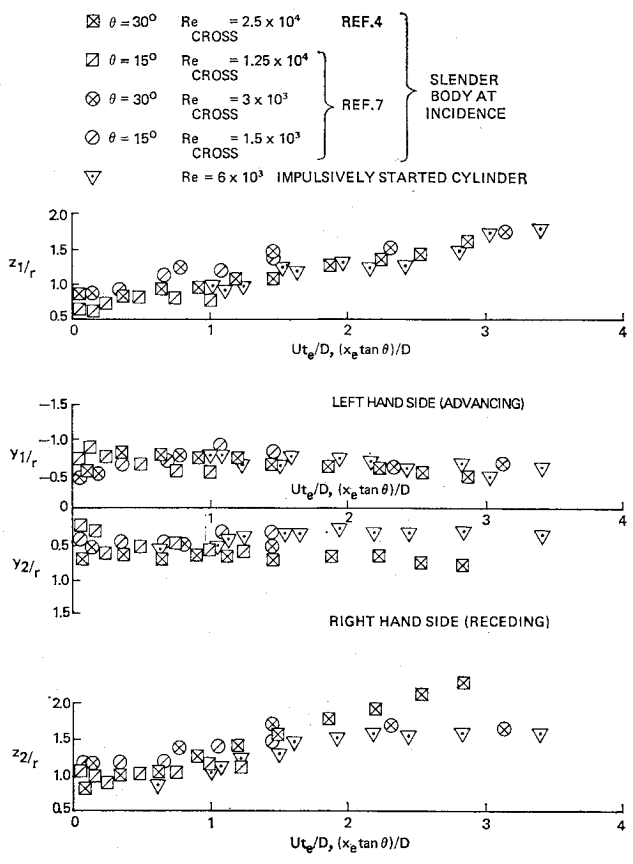

Fig. 6 Variation of vortex position with $(x_e \cdot \tan\theta)/D$ and Ut_e/D for $\alpha = 0.5$.

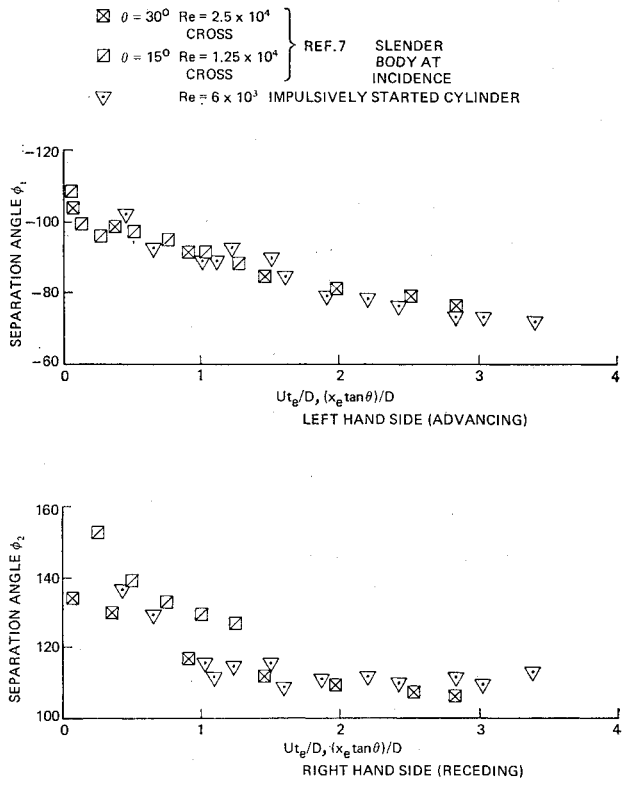

Fig. 7 Variation of separation angle with $(x_e \cdot \tan\theta)/D$ and Ut_e/D for $\alpha = 0.5$.

correlates corresponding separation angles reasonably well[15] at zero incidence, but the correlation progressively deteriorates with the increasing spin ratio. The deterioration may well be connected with the increasing difficulty of measuring separation as the spin ratio increases. A typical variation at $\alpha = 0.5$ is shown in Fig. 7.

In general, the impulsive flow analogy gives a sufficiently accurate correlation to allow the explanation, of the negative Magnus lift force in two-dimensional flow, to be used as the basis for an explanation of the negative Magnus side force experienced by spinning, inclined, slender bodies of revolution.

Application of the Two-Dimensional Explanation to the Three-Dimensional Results

From the explanation of the negative Magnus lift force given above it is to be expected that, for small spin ratios ($\alpha \leqslant 0.5$) in the critical Reynolds number region, the separation angle, on the advancing side of the tangent ogive cylinder, would move in the direction of the cross-flow, i.e., opposite to the spin direction. At $Re_{cross} = 1 \times 10^5$ this certainly happens at all axial stations as is indicated elsewhere.[7] At $Re_{cross} = 2.5 \times 10^4$, i.e. a subcritical Reynolds number, it does not happen, again as one would expect. The separation angle on the receding side of the cylinder is approximately the same for both Reynolds numbers at all axial stations. The results for a typical axial location are shown in Fig. 8.

Generally, just prior to separation the pressure outside the boundary layer is low. From an examination of Fig. 8, a local side force to the left (negative) would be expected at $Re_{cross} = 1 \times 10^5$, through a consideration of the separation angles alone. Following the same reasoning, a local side force to the right (positive) would be expected at $Re_{cross} = 2.5 \times 10^4$. The measured total side force at $Re_{cross} = 1 \times 10^5$ is to the right, with a centre of pressure approximately 75% of the body length from the nose. Consequently the local side force will also be to the right. Similarly, the local side force will be directed to the left at $Re_{cross} = 2.5 \times 10^4$. Thus at both Reynolds numbers, the measured side force is in a direction opposite to that suggested by the separation angles, and hence opposite to that suggested by the two-dimensional explanation.

However, the flow on the leeward side of a slender body at large angles of incidence, is characterised by two vortices, which are aligned approximately parallel to the axis of the body, and which spring from the nose body junction and grow as they move downstream. Each body vortex modifies the pressure distribution on the cylinder, by creating a low pressure region on the cylinder adjacent to itself. The closer and stronger the vortex, the more extensive and intense will be the region of low pressure.

In the situation shown in Fig. 8, it will be the vortices closer to the model surface which will have the greater effect. Thus for $Re_{cross} = 1 \times 10^5$ the body vortex on the right-hand side will be more significant. The ensuing low pressure region over the right rear (in the cross-flow direction) of the model will produce a force in the direction of the measured side force. Similarly, the left-hand vortex will be more effective at $Re_{cross} = 2.5 \times 10^4$, leading to a net force directed to the left.

If the side forces are strongly dependent on the body vortex positions and strengths, as suggested here, then it implies that the spinning, impulsively-started, two-dimensional cylinder will experience a positive Magnus lift force in the critical Reynolds number region at small Ut/D. At large Ut/D, the steady-state results of Swanson[3] must be apporached i.e. a negative Magnus lift force will occur. It is worth noting that Swanson indicates that the negative lift force measured was subjected to a fluctuating force component of the same magnitude as the measured component. This

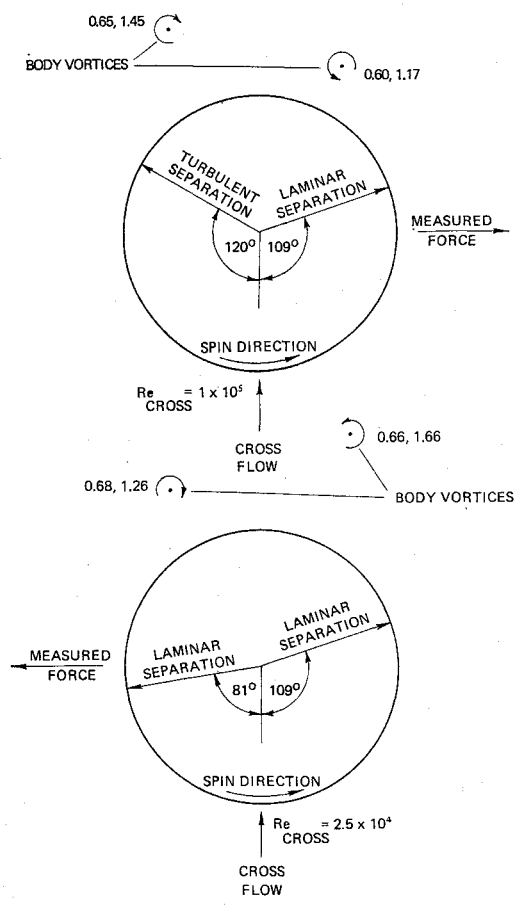

Fig. 8 Comparison of measured separation angle, body vortex position and force direction for a tangent-ogive cylinder at $x/D = 4.55$, $\alpha = 0.44$ and $\theta = 30°$.

implies that the effect of the body vortices being generated and discharged gives rise to the fluctuating force. For a spinning impulsively-started two-dimensional, cylinder at small values of Ut/D, the three-dimensional results suggest that a negative Magnus lift force may be produced at certain subcritical Reynolds numbers.

Theoretical Calculation of the Side Force Associated with the Vortex and Separation Positions

It has been demonstrated that, by including the effects of of the body vortices, the explanation of the two-dimensional Magnus lift force can be applied to a spinning, inclined, body of revolution which is producing a negative Magnus side force.

With the aid of experimentally determined values of vortex and separation positions,[15] it is possible to use potential flow theory to calculate the forces on an impulsively started cylinder,[24] after a nondimensional time Ut/D equivalent to the axial distance $(x \cdot \tan\theta)/D$ along the body. By integrating the instantaneous lift force over the equivalent Ut/D the Magnus side force can be obtained. This can be compared with the side force measured on a tangent-ogive cylinder at large angles of incidence.[4,7]

Potential flow models put forward by other investigators have represented, by various means, those physical characteristics of the flow that are dominated by viscosity, e.g., the separation point, the shed boundary layer and the flow in the wake. For example to represent the shear layer, Bryson[25] has postulated a connecting sheet of vanishingly small vorticity; however this implies a discontinuous change in pressure on the body in crossing the connecting point of the sheet. Gerrard[26] and Oberkampf and Nicolaides[27] have represented the shed boundary layer by a distribution of discrete vortices of small strength. Since the velocity of each vortex has to be computed individually, this approach leads to large computer execution time. For steady flows the wake is usually considered an area of constant pressure and zero velocity and the shear layer becomes a dividing streamline[28] between the freestream and quiescent wake. In the present model the forces on the body are required and the shear layers do not significantly contribute to them, consequently the shear layers have not been specifically represented.

In the wake region close to the surface it is assumed the flow is caused only by the two main vortices and their images, i.e., that it is not influenced by the freestream. This leads to a pressure discontinuity at the separation point; to remove the pressure discontinuity, a correction, which varies linearly between its values at the separation points, is added on in the wake region. Pressure distribution obtained on slender, inclined axisymmetric bodies by the author and those of Ref. 9 suggest that where the vortices are weak or far removed, the pressure across the wake is substantially constant for a nonspinning body. Hence for a spinning body the pressure associated with the nonvortex effects is assumed to vary linearly between its values at the separation points. Use of a different equation for the complex potential in the wake region requires a modification [see Eq. (12)] to Blasius' equation for the forces on the body.

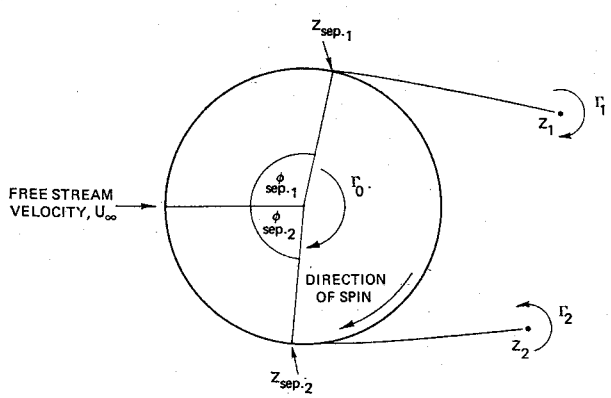

Fig. 9 Theoretical flow model.

The impulsive flow past a two-dimensional circular cylinder at small Ut/D is shown in Fig. 9. The complex potential for such a flow is given by Milne-Thomson[24] as

$$W = (z + 1/z) + (\Gamma_0/2\pi) \cdot \ln z + (i\Gamma_1/2\pi) \cdot [\ln(z - z_1) - \ln(z - 1/\bar{z}_1) + \ln z] + (i\Gamma_2/2\pi) \cdot [\ln(z - z_2) - \ln(z - 1/\bar{z}_2) + \ln z] \quad (3)$$

where the vortex coordinates are nondimensionalised with r, the cylinder radius, and the vortex strengths are nondimensionalized with $U_\infty \cdot r$. Differentiating Eq. (3) with respect to z gives the complex conjugate velocity,

$$\frac{dW}{dz} = u - iv = 1 - \frac{1}{z^2} + \frac{i\Gamma_0}{2\pi z} + \frac{i\Gamma_1}{2\pi}\left(\frac{1}{z - z_1} - \frac{1}{z - 1/\bar{z}_1} + \frac{1}{z}\right) + \frac{i\Gamma_2}{2\pi}\left(\frac{1}{z - z_2} - \frac{1}{z - 1/\bar{z}_2} + \frac{1}{z}\right) \quad (4)$$

The instantaneous forces acting on the cylinder are given by Blasius' theorem,[24] in nondimensional form as,

$$C_D - iC_L = i\left[\frac{1}{2}\oint\left(\frac{dW}{dz}\right)^2 dz - \frac{d}{d\tau}\oint \overline{W} d\bar{z}\right] \quad (5)$$

where $\tau = Ut/r$ and W and z etc. are nondimensionalized as in Eq. (3).

The rate at which circulation from the boundary-layer flows past any plane section of a shear layer is

$$K = \int_0^\delta \left(\frac{\partial v}{\partial x} - \frac{\partial u}{\partial y}\right) \cdot u \cdot dy \quad (6)$$

Since $(\partial v/\partial x)$ is small compared with $\partial u/dy$ the integration gives the approximate result

$$K \approx \tfrac{1}{2}(U^2_{\text{outer}} - U^2_{\text{inner}}) \quad (7)$$

where U_{outer} and U_{inner} are the velocities at the outer and inner edges of the shear layer, respectively. Normally Eq. (7) is applied at separation, and it is assumed that only a certain proportion λ of the discharged circulation reaches the primary vortices,[29] the rest of the discharged circulation being degraded by the effects of viscosity and turbulence. Experiments carried out by Sarpkaya and Garrison[13] indicate that λ is approximately 0.5.

However, Eq. (7) can be applied to any part of the shear layer. Thus Gerrard[26] arbitrarily chose a control surface perpendicular to the freestream direction, and situated one cylinder radius downstream of the circular cylinder. In the present model a control surface perpendicular to the freestream at the end of the shear layer is assumed. At this point the velocity at the outer edge of the shear layer will not be much above the freestream velocity, and the velocity at the inner edge will be close to zero, so that Eq. (7) can be written

$$K \approx \tfrac{1}{2} \cdot U^2{}_\infty \quad (8)$$

Comparing this with the result obtained by Sarpkaya and Garrison,[13] namely

$$K \approx \tfrac{1}{2}(\tfrac{1}{2}U^2\text{sep}) = \tfrac{1}{2}[\tfrac{1}{2}(1.4U_\infty)^2]$$

approximately the same numerical value is obtained. This is to be expected since the control surface is placed after the shear layer which dissipates approximately half of the circulation discharged from the boundary layer. This implies

that, for small spin ratios, the spinning cylinder does not significantly change the strength of the vortices from that produced by a nonspinning cylinder. In nondimensional terms, the main vortex strengths are give by $\Gamma_1 = -\Gamma_2 = 0.5\tau$. This is in keeping with the approximately linear growth for uniformly accelerated cylinders[13] up to $Ut/D = 4$.

In Eqs. (3) and (4) a vortex of strength Γ_0 is placed at the center of the cylinder to represent the cylinders' spin. At the edge of the cylinder (i.e. the inner edge of the boundary layer), the spin is equivalent to a vortex of strength $2\pi\alpha$. In the present model it is assumed that only a small proportion of the spin is transmitted through the boundary layer. Thus the outer, invisced flow "feels" a vortex of strength $\Gamma_0 = 2\pi k \cdot \alpha$ at the origin. From Ref. 3 it is deduced that $k \approx 0.05$. Thus the primary effect of the spin on the outer flow is the marked shift in boundary-layer separation positions. This in turn causes the vortices to take up an asymmetric pattern. The asymmetric vortex positions and the asymmetric separation positions in turn generate an asymmetric pressure distribution on the body, which results in a residual lift force.

In the region close to the cylinder surface immediately after separation the flow is not affected by the freestream. Therefore, in calculating the surface velocity and pressure, it is appropriate to ignore the freestream and doublet term, $1 - 1/z^2$, in the separated flow region. This leads to a discontinuity in pressure coefficient at the separation position equal to

$$\Delta C_P = \tfrac{1}{2}(U^2\text{sep} - [U\text{sep} - 2\sin(\theta\text{sep})]^2) = 2.\sin(\theta\text{sep}).[U\text{sep} + \sin(\theta\text{sep})]. \quad (9)$$

Since such a discontinuity is physically unrealistic, ΔC_P is subtracted from the calculated values of C_P (due to vortices) in the separated flow region. In general, for the spinning cylinder, the correction ΔC_P obtained from the two separation positions will be different. It assumed is that ΔC_P varies linearly between its values at the separation positions, i.e.,

$$\Delta C_P = \Delta C_{P_1} + [(\varphi - \varphi_{\text{sep}_1}/\varphi_{\text{sep}_2} - \varphi_{\text{sep}_1})].(\Delta C_{P_2} - \Delta C_{P_1})$$

The correction to the over-all force coefficient is then given by

$$\Delta(C_D - i \cdot C_L) = \frac{-1}{2} \cdot \int_{\varphi_{\text{sep}_1}}^{\varphi_{\text{sep}_2}} \Delta C_P.(\cos\varphi - i\sin\varphi)d\varphi$$

which can be evaluated to give

$$\Delta C_D = \frac{1}{2} \cdot \left[\frac{(\Delta C_{P_1} \cdot \varphi_{\text{sep}_2} - \Delta C_{P_2} \cdot \varphi_{\text{sep}_1})}{(\varphi_{\text{sep}_2} - \varphi_{\text{sep}_1})} \cdot (\sin\varphi_{\text{sep}_1} - \sin\varphi_{\text{sep}_2}) \right.$$
$$\frac{-(\Delta C_{P_2} - \Delta C_{P_1})}{(\varphi_{\text{sep}_1} - \varphi_{\text{sep}_2})} \cdot (\cos\varphi_{\text{sep}_2} - \cos\varphi_{\text{sep}_1} + \varphi_{\text{sep}_2} \cdot \sin\varphi_{\text{sep}_2} -$$
$$\left. \varphi_{\text{sep}_1} \cdot \sin\varphi_{\text{sep}_1}) \right] \quad (10)$$

and

$$\Delta C_L = \frac{1}{2} \cdot \left[\frac{(\Delta C_{P_1} \cdot \varphi_{\text{sep}_2} - \Delta C_{P_2} \cdot \varphi_{\text{sep}_1})}{(\varphi_{\text{sep}_2} - \varphi_{\text{sep}_1})} \cdot (\cos\varphi_{\text{sep}_2} - \cos\varphi_{\text{sep}_1}) \right.$$
$$\frac{-(\Delta C_{P_2} - \Delta C_{P_1})}{(\varphi_{\text{sep}_2} - \varphi_{\text{sep}_1})} \cdot (\sin\varphi_{\text{sep}_2} - \sin\varphi_{\text{sep}_1} + \varphi_{\text{sep}_1} \cdot \cos\varphi_{\text{sep}_1} -$$
$$\left. \varphi_{\text{sep}_2} \cdot \cos\varphi_{\text{sep}_2}) \right] \quad (11)$$

In evaluating Eq. (5) it is necessary to use the modified complex velocity, $dW/dz - (1 - 1/z^2)$, in the separated flow region. Since the term $(1 - 1/z^2)$ is a steady flow term, there is no modification to the second part of Eq. (5), the unsteady force contribution. The first term in Eq. (6) becomes

$$\frac{-i}{2}\oint (u - iv)^2 dz = \frac{i}{2}\left[\int_{ei\cdot 0}^{z_{\text{sep}_1}} \left(\frac{dW}{dz}\right)^2 dz + \int_{z_{\text{sep}_1}}^{z_{\text{sep}_2}} \left[\left(\frac{dW}{dz}\right) - \right.\right.$$
$$\left. (1 - 1/z^2) \right]^2 dz + \int_{z_{\text{sep}_2}}^{e^{i2\pi}} \left(\frac{dW}{dz}\right)^2 dz \Big] = \frac{1}{2}\left[\oint \left(\frac{dW}{dz}\right)^2 dz - \right.$$
$$\left. \int_{z_{\text{sep}_1}}^{z_{\text{sep}_2}} (1 - 1/z^2) \cdot \left(2\frac{dW}{dz} - (1 - 1/z^2) \right) dz \right],$$

where z_{sep_1} is the complex position corresponding to the separation angle θ_{sep_1}. Thus the second term is the correction to the steady Blasius force due to omitting the freestream and doublet term in the separated flow region. Let this correction be χ.

$$\chi = \frac{i}{2}\left[[z + 2/z - 1/3z^3 - 2(1 - 1/z^2) \cdot W]_{z_{\text{sep}_1}}^{z_{\text{sep}_2}} + \right.$$
$$\left. 4 \cdot \int_{z_{\text{sep}_1}}^{z_{\text{sep}_2}} W/z^3 dz \right]$$

which on evaluation, substitution for W and simplification yields

$$\chi = \frac{i}{2}\left[[-z - 2/z + 1/3z^3 + ik \cdot \alpha \cdot (2\ln z + 1/z^2)]_{z_{\text{sep}_1}}^{z_{\text{sep}_2}} + \right.$$
$$\frac{i\Gamma_1}{\pi}\left[\ln(z - z_1) \cdot (-1 + 1/z_1^2) + \ln(z - 1/\bar{z}_1) \cdot (1 - \bar{z}_1^2) - \right.$$
$$\left. \ln z \cdot (1 + 1/z_1^2 - \bar{z}_1^2) + \frac{1}{z}(1/z_1 - \bar{z}_1 - 1/2z) \right]_{z_{\text{sep}_1}}^{z_{\text{sep}_2}} +$$
$$\frac{i\Gamma_2}{\pi}\left[\ln(z - z_2) \cdot (-1 + 1/z_2^2) + \ln(z - 1/\bar{z}_2) \cdot (1 - \bar{z}_2^2) - \right.$$
$$\left. \left. \ln z \cdot (1 + 1/z_2^2 - \bar{z}_2^2) + \frac{1}{z}(1/z_2 - \bar{z}^2 - 1/2z) \right]_{z_{\text{sep}_1}}^{z_{\text{sep}_2}} \right]. \quad (12)$$

Sarpkaya[30] evaluates

$$\frac{1}{2}\oint \left(\frac{dW}{dz}\right)^2 dz - \frac{d}{d\tau}\oint \bar{W} d\bar{z}$$

by modifying Lagally's theorem to give the forces in terms of the vortex velocities which can be easily obtained by putting $z = z_1, z_2$ in Eq. (4). This gives

$$C_D = +\Gamma_1 \cdot (v_1 - v_{i_1}) + \Gamma_2 \cdot (v_2 - v_{i_2}) - y_{i_1} \cdot \dot{\Gamma}_1 - y_{i_2} \cdot \dot{\Gamma}_2 \quad (13)$$

$$C_L = +\Gamma_1(1 - u_1 + u_{i_1}) + \Gamma_2(1 - u_2 + u_{i_2}) + x_{i_1} \cdot \Gamma_1 + x_{i_2} \cdot \Gamma_2 \quad (14)$$

where x_i and y_i are the coodinates of the image vortex, and u_i and v_i are the velocity components of the image vortex, which are given by

$$\left[\frac{d\bar{W}}{d\bar{z}}\right]_{z=z_i} = -\left[\frac{dW}{dz}\right] \Big/ \bar{z}^2 \quad (15)$$

At each axial station, $(x \cdot \tan\theta)/D$, Eqs. (10) to (14) can be evaluated to give the overall local lift coefficient on the section, in terms of the measured vortex and separation positions. By integrating the side force along the axsymmetric body, the total side force is obtained.

The computed total side forces are shown in Fig. 10 for angles of incidence, 15 and 30°, and for cross-flow Reynolds numbers in the range 1.25×10^4 to 1×10^5. It is apparent that qualitative agreement has been obtained. In general the predicted side force is more sensitive to small changes in separation angle than in vortex position or strength. The finite values of C_Y at $\alpha = 0$ in Fig. 10 are due to using

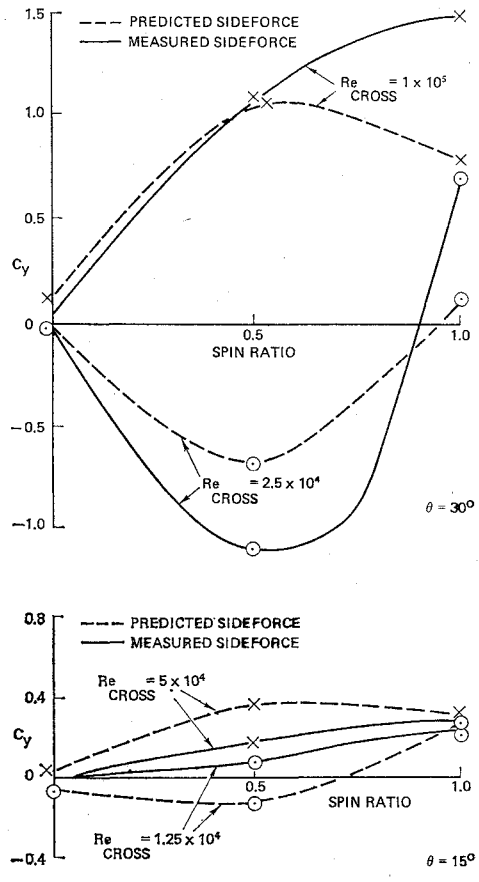

Fig. 10 Comparison of measured and predicted side force.

experimental values of the vortex and separation positions.

As indicated previously, a spinning, impulsively started two-dimensional cylinder might be expected to produce a negative Magnus lift force at small values of Ut/D for certain subcritical Reynolds numbers. By applying the theoretical model, described above, to the separation angles and body vortex positions measured in the wake of a spinning, impulsively started two-dimensional cylinder it has been possible to predict the Magnus lift force development with Ut/D. However the results[15] did not indicate a large negative Magnus force. This is not surprising since the Reynolds number of the two-dimensional test was 6×10^3, whereas the cross-flow Reynolds number at which the negative Magnus side force occurred was 2.5×10^4, and further that the vortex positions at equivalent values of Ut_e/D and $(x_e \cdot \tan\theta)/D$ for cross-flow Reynolds numbers 6×10^3 did not agree with those for 2.5×10^4 (see Fig. 6). The negative lift force may well be connected with the occurrence of tertiary vortices which are present[7] at $Re_{cross} = 2.5 \times 10^4$.

Since the separation positions are in qualitative agreement with those measured for steady flow (i.e., any induced vortex effects on the separation positions are averaged out) about a spinning two-dimensional cylinder[5] at comparable Reynolds numbers, it seems plausible to suggest that the precise location of the separation positions are principally a function of the boundary-layer development around a spinning cylinder, and that any perturbations in the pressure distribution caused by the vortices, have only a small effect on the separation positions. Given the asymmetric separation positions, it has been shown that this alone would lead one to expect a positive Magnus side force at subcritical Reynolds numbers. In practice, a negative Magnus side force occurs due to the particular vortex locations adopted (see Fig. 8).

Given an arbitrary separation configuration, the question remains: why do the vortices adopt a particular pattern? One can only suggest that the vortices are forced to adopt a pattern defined by some overall stability condition similar to the Foppl condition for zero spin.[31]

Conclusion

It has been demonstrated that the explanation of the negative Magnus lift force, experienced by a spinning two-dimensional cylinder, can be meaningfully applied to the Magnus side force experienced by a spinning slender body of revolution at large angles of incidence, if proper account is taken of the body vortices. In fact, the body vortices cause a positive Magnus side force where the two-dimensional explanation would lead one to expect a negative side force. However, the location of the body vortices appears to be prescribed by the particular separation position configuration adopted.

References

[1] Tani, I., "Low-Speed Flows Involving Bubble Separations," *Progress in Aeronautical Science*, edited by D. Kuchemann, Vol. 5, Pergamon Press, Oxford, 1965, pp. 70–103.

[2] Krahn, E., "Negative Magnus Force," *Journal of Aeronautical Sciences*, Vol. 23, No. 4, April 1956, pp. 377–378.

[3] Swanson, W. M., "An Experimental Investigation of the Magnus Effect," Final Rept., OOR Project 1082, Dec. 1956, Case Inst. of Technology, Cleveland., Ohio.

[4] Fletcher, C. A. J., "Investigation of the Magnus Characteristics of a Spinning Inclined Ogive-Cylinder Body at M = 0.2," TN HSA 159, Oct. 1969, Weapons Research Establishment, Salisbury, South Australia.

[5] Griffiths, R. T., and Ma, C. X., "Differential Boundary-Layer Separation Effects in the Flow Over a Rotation Cylinder," *Journal of the Royal Aeronautical Society*, Vol. 73, No. 702, June 1969, pp. 524–526.

[6] Allen, H. J., and Perkins, E. W., "A Study of the Effects of Viscosity on flow Over Slender Inclined Bodies of Revolution," Rept. 1048, 1951, NACA.

[7] Fletcher, C. A. J., "The Magnus Characteristics of a Spinning Inclined Ogive-Cylinder Body at Subcritical Reynolds Numbers in Incompressible Flow," Rept. 423, (WR&D), July 1971, Weapons Research Establishment, Salisbury, South Australia.

[8] Roshko, A., "Experiments on the Flow Past a Circular Cylinder at very High Reynolds Numbers," *Journal of Fluid Mechanics*, Vol. 10, No. 3, May 1961, pp. 345–356.

[9] Tinling, B. E. and Allen, C. Q., "An Investigation of the Normal-Force and Vortex-Wake Characteristics of an Ogive-Cylinder Body at Subsonic Speeds," TN D-1297, April 1962, NASA.

[10] Schlicting, H., "*Boundary Layer Theory*," 1st English ed., McGraw-Hill, New York, 1955, p. 184.

[11] Sarpkaya, T., "Separated Flow about Lifting Bodies and Impulsive Flow About Cylinders," *AIAA Journal*, Vol. 4, No. 3, March 1966, pp. 414–420.

[12] Prandtl, L. and Tietjens, O. G., "*Applied Hydro-and Aeromechanics*," 1st ed. McGraw-Hill, New York, 1934, p. 270.

[13] Sarpkaya, T. and Garrison, C. J., "Vortex Formation and Resistance in Unsteady Flow," *Transactions of the ASME, Ser. E: Journal of Applied Mechanics*, Vol. 30, No. 1, March 1963, pp. 16–24.

[14] Asher, J. A. and Dosanjh, D. S., "An Experimental Investigation of the Formation and Flow Characteristics of an Impulsively Generated Vortex Street," *Transactions, of the ASME, Ser. D: Journal of Basic Engineering*, Vol. 90, No. 4, Dec. 1968, pp. 596–606.

[15] Fletcher, C. A. J., "An Explanation of the Negative Magnus Side Force Experienced by a Spinning, Inclined Ogive-Cylinder," TN 489(WR&D), Nov. 1971, Weapons Research Establishment, Salisbury, South Australia.

[16] Jorgensen, L. H. and Perkins, E. W., "Investigation of Some Wake Vortex Characteristics of an Inclined Ogive-Cylinder Body at Mach Number 2," Rept. 1371, 1958, NACA.

[17] Raney, D. J., "Measurement of the Cross-Flow around an Inclined Body at Mach Number of 1.91," TN Aero, 2357, Jan. 1957, Royal Aircraft Establishment, Farnborough, Hants, England.

[18] Grosche, F. R., "Windkanaluntersuchung des Wirbelsystems an einem angestellten schlanken Rotationskörper ohne und mit Tragflugel," *Zeitsehrift Flugwiss*, Vol. 18, No. 6, 1970, pp. 208–217.

[19] Nielsen, J. N., *Missile Aerodynamics*, 1st ed., McGraw-Hill, New York, 1960, pp. 87–89.

[20] Greene, J. E., "Static Stability and Magnus Characteristics of the 5-Caliber and 7-Caliber Army-Navy Spinner Rocket at Low Subsonic Speeds," NAVORD Rept. 3884, Dec. 1954, U.S. Naval Ordnance Lab., White Oak, Md.

[21] Thomson, K. D. and Morrison, D. F., "The Spacing, Position and Strength of Vortices in the Wake of Slender Cylindrical Bodies at Large Incidence," Rept. HSA 25, June 1969, Weapons Research Establishment, Salisbury, South Australia.

[22] Thomson, K. D. and Morrison, D. F., "The Spacing, Position and Strength of Vortices in the Wake of Slender Cylindrical Bodies at Large Incidence," *Journal of Fluid Mechanics*, Vol. 50, Pt. 4, June 1971, pp. 751–783.

[23] Marshall, F. J., "Impulsive Motion of a Cylinder and Viscous Cross-Flow," *Journal of Aircraft*, Vol. 7, No. 4, July 1079, pp. 371–373.

[24] Milne-Thomson, L. M., *Theoretical Hydrodynamics*, 3rd ed., MacMillan, London, 1955, p. 354.

[25] Bryson, A. E., "Symmetric Vortex Separation on Circular Cylinders and Cones," Transactions *of the ASME, Ser. E: Journal of Applied Mechanics*, Vol. 26, No. 4, Dec. 1959, pp. 643–648.

[26] Gerrard, J. H., "Numerical Computation of the Magnitude and Frequency of the Lift on a Circular Cylinder," *Proceedings of the Royal Society, Ser. A*, Vol. 261, No. 18, Jan. 1967, pp. 137–162.

[27] Oberkampf, W. L. and Nicolaides, J. D., "Aerodynamics of Finned Missiles at High Angle of Attack," *AIAA Journal*, Vol. 9, No. 12, Dec, 1971, pp. 2378–2384.

[28] Roshko, A., "A New Hodigraph for Free-Streamline Theory," TN 3168, July 1954, NACA.

[29] Roshko, A., "On the Drag and Shedding Frequency of Two-Dimensional Bluff Bodies," TN 3169, July 1954, NACA.

[30] Sarpkaya, T., "Lift Drag,, and Added-Mass Coefficients for a Circular Cylinder Immersed in a Time-Dependent Flow," *Transactions of the ASME, Ser. E: Journal of Applied Mechanics*, Vol. 30, No. 1, March 1963, pp. 13–15.

[31] Seath, D. D., "Equilibrium Vortex Position," *Journal of Spacecraft*, Vol. 8, No. 1, Jan. 1971, pp. 72–75.